Available online at www.sciencedirect.com
ScienceDirect
Journal of Molecular Structure 871 (2007) 131–139
Journal of MOLECULAR STRUCTURE
www.elsevier.com/locate/molstruc

Formation of *N*,*N*,*N*′,*N*′-tetramethylformamidinium disulphide from the chemical and electrochemical oxidation of tetramethylthiourea: Vibrational spectra and crystal structure of the chloride dihydrate salt

A.E. Bolzán [a,*], J.A. Güida [b], R.C.V. Piatti [a], A.J. Arvia [a], O.E. Piro [c], J.R. Sabino [e,d], E.E. Castellano [d]

[a] *Instituto de Investigaciones Fisicoquímicas Teóricas y Aplicadas (INIFTA, CONICET-UNLP), Sucursal 4, Casilla de Correo 16, 1900 La Plata, Argentina*
[b] *CEQUINOR (CONICET-UNLP), Depto. de Quimica, Facultad de Ciencias Exactas and Facultad de Ingeniería, Universidad Nacional de La Plata, 47 esq. 115, CC 962, 1900 La Plata and Depto. de Ciencias Básicas, Universidad Nacional de Luján, Luján, Argentina*
[c] *Depto. de Física, Facultad de Ciencias Exactas, Universidad Nacional de La Plata and IFLP (CONICET), CC 67, 1900 La Plata, Argentina*
[d] *Instituto de Física de São Carlos, Universidade de São Paulo, CP 369, 13560 São Carlos (SP), Brazil*
[e] *Instituto de Física, Universidade Federal de Goiás, CP 191, Goiânia (GO), Brazil*

Received 14 August 2006; received in revised form 31 January 2007; accepted 2 February 2007
Available online 16 February 2007

Abstract

The *N*,*N*,*N*′,*N*′-tetramethylformamidinium disulphide (TMFDS) was prepared from either the electro-oxidation of tetramethylthiourea (TMTU) on platinum electrodes in aqueous perchloric acid solution or the chemical oxidation of TMTU with hydrogen peroxide in hydrochloric acid-containing absolute ethanol. The electrochemical formation of TMFDS at different potentials was followed by *in situ* FTIRRAS spectroscopy. The IR and Raman spectra of TMFDS chemically formed as a chloride dihydrate were determined and compared to the product produced electrochemically. The crystal structure of the chloride salt $[N(CH_3)_2]_2C{=}S{-}S{=}C\,[N(CH_3)_2]_2Cl_2{\cdot}2H_2O$, as determined by X-ray diffraction, crystallises in the monoclinic $C2/c$ space group with $a = 23.267(1)$, $b = 10.824(1)$, $c = 17.774(1)$ Å, $\beta = 126.91(1)°$, and $Z = 8$. The structure was solved from 2489 reflections with $I > 2\sigma(I)$ and refined to an agreement $R1$-factor of 0.0405. The two molecular halves of the dimeric $[N(CH_3)_2]_2C{=}S{-}S{=}C[N(CH_3)_2]_2^{2+}$ ion are linked by a disulphide single bond [d(S—S) = 2.0454(9) Å] and related to each other by a non-crystallographic pseudo two-fold axis. DFT structure optimisation and normal mode frequencies were calculated using the 6-311G(d,f) basis set at DFT theory level. An estimation of the free energy for the dimer formation and rate ratio for the homogeneous and heterogeneous processes are presented. These data are consistent with the electrochemical mechanism of the anodic formation of $TMFDS^{2+}$ from TMTU electro-oxidation in acid solutions.

Keywords: Tetramethylthiourea; DFT; Vibrational spectra; Crystal structure; Oxidation; Formamidinium disulphide; Electrochemistry

1. Introduction

The oxidation of thioureas, a versatile although complex oxidation process in organic chemistry, produces a variety of substances depending on the substitution pattern of the thiourea, the oxidizing agent, the polarity of the medium and other experimental conditions [1]. Accordingly, this type of reaction conveys to either ureas, formamidinium disulphides, formamidinesulphinic acids, formamidinesulphonic acids, 1, 2, 4-thiadiazoles or different benzothiazole derivatives [1,2].

From the electrochemical standpoint, the importance of thiourea (TU) and substituted thioureas arises from their use as additives for metal electroplating [3–8] and metal corrosion inhibition [9], as in the case of protective films of TU derivatives that have been proposed as corrosion inhibitors in nuclear reactors [10,11]. Furthermore, TU and tetramethylthiourea (TMTU) have also been investi-

* Corresponding author. Tel.: +54 221 4257430; fax: +54 221 4254642.
E-mail address: aebolzan@inifta.unlp.edu.ar (A.E. Bolzán).

0022-2860/$ - see front matter © 2007 Elsevier B.V. All rights reserved.
doi:10.1016/j.molstruc.2007.02.004

gated as possible lixiviants for gold recovery from minerals [12–15] by electrodissolving gold as complex species [16,17]. In these processes, the first electro-oxidation stage of thioureas appears to be the formation of a formamidinium disulphide (FDS). For TU and TMTU, FDS and tetramethylformamidinium disulphide (TMFDS), respectively, can also be obtained by homogeneous chemical oxidation using hydrogen peroxide [18,19].

The identification of oxidation products from the electrochemical oxidation of TMTU is rather scarce. In principle, as the anodic potential is increased, a number of products are formed, such as TMFDS, CO_2 and sulphate ions [20], their relative yield depending on the applied potential. In this case, no data on the structure and spectral features of TMFDS were found in the literature, except for a few references that are basically related to the synthesis of coordination compounds [19,21].

This paper reports data on the electrochemical and chemical formation of TMTDS. In the former case, the voltammetric behaviour of the anodic and cathodic processes on platinum provides information about the kinetic behaviour of the overall reaction over a wide range of electric potentials. The crystal structure and spectroscopic characterization of TMFDS as *N*,*N*,*N*′,*N*′-tetramethylformamidinium chloride dihydrate produced by chemical oxidation of TMTU were also determined. Spectroscopic data from both the TMFDS soluble product detected by *in situ* FTIRRAS measurements during the electrochemical oxidation of TMTU in deuterium oxide acid solutions and the TMFDS chloride resulting from chemical oxidation of TMTU are compared. Results from this work throw further light on the mechanism of the electrochemical behaviour of TMTU in aqueous acids pointing out the qualitative validity of a common electrochemical kinetics and mechanism for the first electro-oxidation stage of thioureas on platinum metals in aqueous environments at low anodic potentials ($E < 0.9$ V versus SHE) producing a disulphide.

2. Experimental

2.1. Preparation of TMFDS

TMFDS was electrochemically produced by voltammetric oxidation of TMTU on a platinum electrode at 0.05 V s^{-1} between 0.1 and 0.95 V (versus Standard Hydrogen Electrode (SHE)) at room temperature. For this purpose a conventional three electrode cell with a polycrystalline platinum disc working electrode (0.12 cm^2 geometric area, J. Matthey, spec pure) and a large platinum sheet (2 cm^2 geometric area) as counter electrode was used. The working electrode, used either under quiescent condition or at 2000 rpm rotation speed, was polished with alumina and rinsed with Milli-Q* water before each run. A mercurous sulphate electrode was used as reference, but the potentials in the text are referred to the SHE scale.

The chemical preparation of TMFDS has been described in Ref. [19]. Briefly, 10.57 g (80 mmol) of TMTU were dissolved in 200 ml of ethanol absolute and then 8.1 ml HCl 36% was added. To this solution, kept in an ice bath, 4.6 ml of 30% H_2O_2 was added by dropping. Subsequently, the solution was left at room temperature and the solvent evaporated under vacuum until the volume of the solution was reduced to 50 ml. The remaining solution was cooled down to 4 °C for 4 days to precipitate the solid crystals. Then, the crystals were filtered out, washed with ether and eventually dried in a conventional desiccator containing P_2O_5.

2.2. FTIRRAS experiments

The products from TMTU electro-oxidation were identified by *in situ* Fourier Transform Infrared Reflection Absorption Spectroscopy (FTIRRAS), employing a spectroelectrochemical cell with a 60° prismatic calcium fluoride window that was fitted to a Nicolet Nexus 670 spectrometer equipped with a liquid nitrogen-cooled MCT detector. A platinum disc working electrode (0.7 cm in diameter) mirror-polished with alumina suspension (0.3 μm grit), rinsed with Milli-Q* water, was utilised. The potential of the working electrode was monitored by means of a Wenking 72L potentiostat coupled to a potential step generator. The normalised reflectance spectra were expressed as the ratio R/R_0, where R is the value of the reflectance at the sampling potential E_s and R_0 is the reflectance measured at the reference potential E_{ref}. The value of E_{ref} was set at 0.05 V, a potential where no TMTU electrooxidation occurred, and then increased stepwise up to 1.4 V. Accordingly, as the value of E was changed positively with respect to E_{ref}, negative- and positive-going IR absorption bands in the spectra indicate the formation of new species in and the disappearance of species from the solution, respectively. Spectra were obtained by collecting 256 interferograms with 8 cm^{-1} resolution using parallel (p) polarised light produced by means of a barium fluoride supported aluminum-wire grid polariser. To avoid the possible interference of water bands masking those related to the formation of TMTFDS, runs in deuterium oxide solution were made.

Working solutions were prepared from TMTU (Fluka, puriss.), perchloric acid (70% Alfa Aesar) and either Milli-Q* water or deuterium oxide (Aldrich, 99.9%), and continuously kept under nitrogen saturation during the experiments. Runs were made at 298 K.

2.3. X-ray diffraction data

Single crystal X-ray data were collected on an Enraf-NoniusKappa CCD diffractometer using MoKα radiation ($\lambda = 0.71073$ Å). Crystal data and refinement results are summarized in Table 1. Data collection: COLLECT [22]. Cell refinement and data reduction: DENZO and SCALEPACK [23]. The structure was solved by direct methods with SHELXS [24] and its non-H atom refined by full-matrix least-squares based on $F2$ with SHELXL [25]. The

Table 1
Crystal data and structure refinement results for $[N(CH_3)_2]_2C{=}S{-}S{=}C[N(CH_3)_2]_2Cl_2.2H_2O$

Chemical formula	$C_{10}H_{28}Cl_2N_4O_2S_2$
Formula weight	371.38
Temperature (K)	293(2)
Crystal system	Monoclinic
Space group	*C*2/*c* (No. 15)
a, *b*, *c* (Å)	23.267(1), 10.824(1), 17.774(1)
β (°)	126.91(1)
Volume (Å^3)	3579.1(4)
Z, calculated density (mg/m^3)	8, 1.378
Crystal size (mm)	$0.15 \times 0.15 \times 0.20$
Absorption coefficient (mm^{-1})	0.603
Crystal color/shape	Colorless/fragment
Radiation, graphite monochr.	MoKα, $\lambda = 0.71073$ Å
θ range for data collection (°)	2.87–26.35
Index ranges	$-28 \leqslant h \leqslant 28$, $-13 \leqslant k \leqslant 10$, $-22 \leqslant l \leqslant 22$
Reflections collected/unique	11507/3624 [R(int) = 0.0498]
Observed reflections [$I > 2\sigma(I)$]	2489
Completeness (%)	99.5 (to $\theta = 26.35$)
Refinement method	Full matrix least squares on F^2
Weights, *w*	$[\sigma^2(F_o^2) + (0.0514P)^2]^{-1}$ $P = [\mathrm{Max}(F_o^2, 0) + 2F_c^2]/3$
Data/restraints/parameters	3614/0/205
Goodness-of-fit on F^2	1.003
Final *R*-index [$I > 2\sigma(I)$][e]	$R1 = 0.0405$, $wR2 = 0.0900$
R indices (all data)	$R1 = 0.0718$, $wR2 = 0.1043$
Largest peak and hole (e A^{-3})	0.257 and −0.286

Least-squares refinement of the angular settings for 11507 reflections in the $2.87 < \theta < 26.35°$ range.
[e] *R*-Indices defined as: $R_1 = \Sigma||F_o| - |F_c||/\Sigma|F_o|$, $wR_2 = \left[\Sigma w(F_o^2 - F_c^2)^2 / \Sigma w(F_o^2)^2\right]^{1/2}$.

$[N(CH_3)_2]_2C{=}S{-}S{=}C[N(CH_3)_2]_2^{2+}$ methyl hydrogen atoms were positioned stereo-chemically and refined with the riding model by considering the CH_3 as rigid groups allowed to rotate around the corresponding C=N bond. The H-atoms of the two crystallisation water molecules were located in a difference Fourier map and refined isotropically at their found positions. The molecular drawing was obtained with ORTEP [26].

2.4. Vibrational spectroscopy

Infrared spectra of samples (as KBr pellets) were recorded with an FTIR Bruker 113v spectrophotometer equipped with a mid IR DTGS detector working at 2 and 4 cm^{-1} resolution. Raman spectra were obtained with the same resolutions at room temperature utilising an FTIR Bruker 66 spectrophotometer fitted with an NIRR attachment.

3. Results and discussion

3.1. Electrochemical formation of TMFDS

The voltammetric electro-oxidation of TMTU in quiescent aqueous 1 mM TMTU + 0.1 M sulphuric acid at 0.05 V s^{-1}, between 0.05 and 1.0 V (Fig. 1a), shows an anodic current peak at 0.68 V (peak *Ia*) assigned to the formation of TMFDS [20]. The reverse scan shows a cathodic peak at 0.27 V (peak *Ic*) that corresponds to the electroreduction of the anodically formed product TMFDS to TMTU. This voltammogram resembles that of TU electro-oxidation on platinum yielding FDS [27]. For the working electrode rotated at 2000 rpm (Fig. 1b) the voltammogram shows that peak *Ia* is largely depressed and only a small shoulder during the positive potential scan can be seen, whereas peak *Ic*, appearing during the negative potential scan, is suppressed. These features indicate that both anodic and cathodic processes are under diffusion control, the reacting species anodically formed being swept out from the electrode—solution interface.

To identify the anodic product from the electro-oxidation of TMTU, the IR spectra were recorded *in situ* at different applied potentials. To avoid any interference of water bands, TMTU electro-oxidation was carried out in deuterium oxide solution.

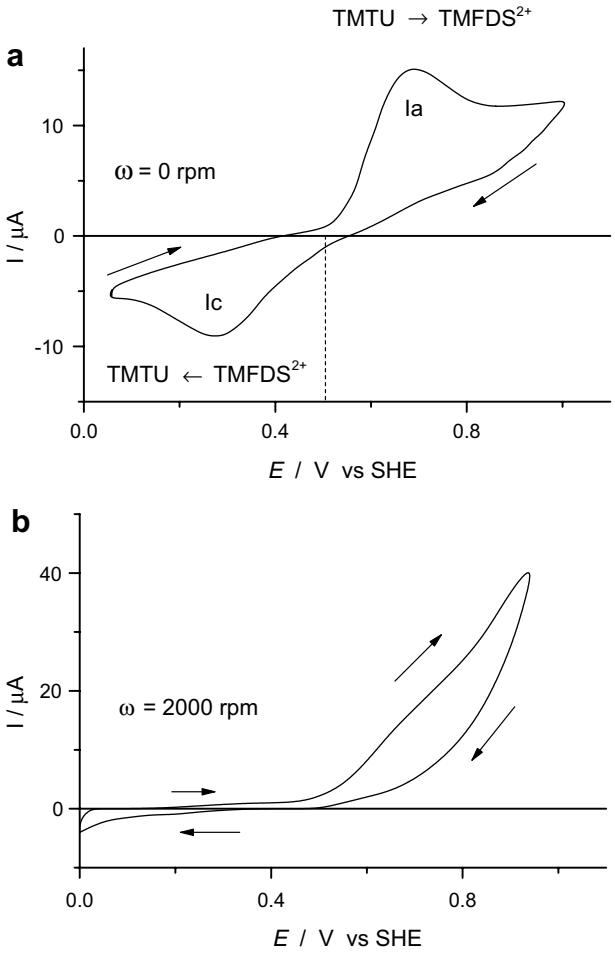

Fig. 1. Stabilised voltammograms for the electro-oxidation of TMTU on platinum from 1 mM TMTU + 0.1 M perchloric acid run at 0.05 V s^{-1}. (a) In quiescent solution. The vertical line indicates the mean half-wave anodic/cathodic potential values of the redox couple; (b) The same as in (a) under rotation at 2000 rpm. Note the absence of faradaic cathodic current in the reverse scan. $T = 298$ K

The FTIRRAS spectra show the formation of electro-oxidation products from $E = 0.5$ V upwards (Fig. 2), the intensity of the bands increasing with E. Positive bands correspond to the disappearance of TMTU from the anode solution layer, whereas negative bands reveal the appearance of products such as TMTFDS. For $E = 0.5$ V and $E = 0.7$ V, bands at 1236, 1373 and 1537 cm^{-1} are assigned to the disappearance of TMTU [16,28], and the negative bands at 1171, 1405, 1460 and 1623 cm^{-1} are related to $TMFDS^{2+}$ [19,20], the first electro-oxidation product from TMTU. For $E = 1.4$ V, a new negative band at 1700 cm^{-1}, a wavenumber typically related to carbonyl-containing species, is observed. This band indicates that at sufficiently positive potentials, a second electro-oxidation stage of TMTU sets in. Previous results obtained at $E > 1.4$ V have shown the appearance of bands at 1200 and 2343 cm^{-1} together with the band at 1700 cm^{-1} indicating that further electro-oxidation of either TMTU or $TMFDS^{2+}$ yields oxygen-containing products such as CO-containing species, CO_2 and SO_4^{2-} ions [20].

In conclusion, the first TMTU electro-oxidation stage occurring in the range 0.5–1.2 V seemingly yields $TMFDS^{2+}$ as the main product. To provide unequivocal support to this conclusion, the IR spectrum of solid $TMFDS^{2+}$ salt was investigated after the crystal structure was determined.

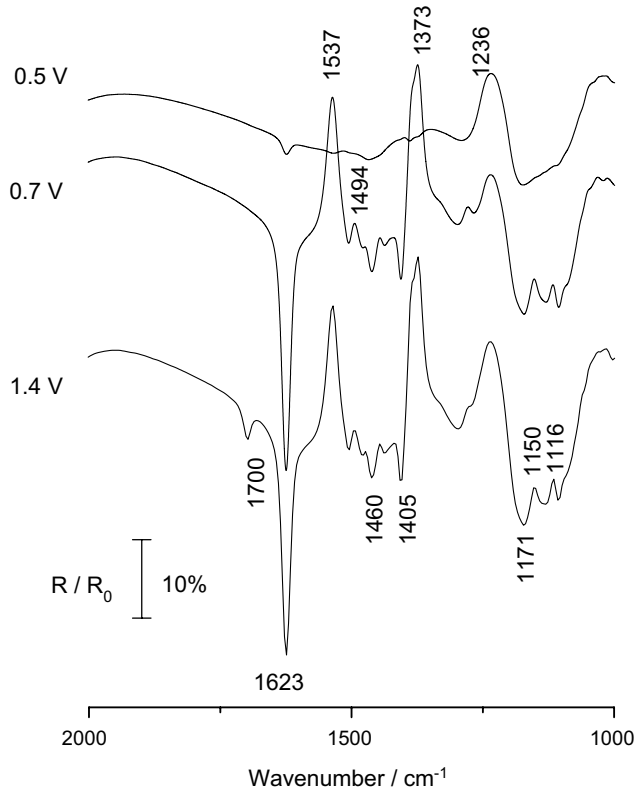

Fig. 2. *p*-Polarised light FTIRRAS spectra of TMTU electro-oxidation on platinum at different potentials as indicated. 0.1 M TMTU + 0.1 M perchloric acid in deuterium oxide. $E_{ref} = 0.05$ V.

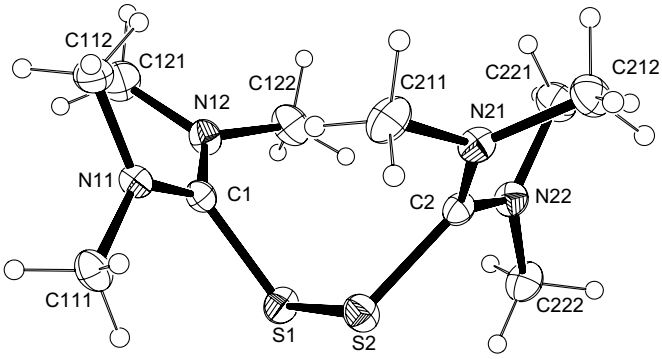

Fig. 3. A view of the TMFDS cation showing the labelling of the non-H atoms and their displacement ellipsoids at the 50% probability level. The local twofold axis is along the vertical through the mid point of the disulphide S—S bond.

3.2. Crystal structure of TMFDS

Fig. 3 shows a molecular diagram of the $[N(CH_3)_2]_2C{=}S{-}S{=}C[N(CH_3)_2]_2^{2+}$ ion. Selected intra-molecular bond distances and angles are reported in Table 2. The organic ion can be described as a tetramethylformamidinium dimer linked through a disulphide single bond (d(S—S) = 2.0454(9) Å). The bonding re-arrangement produces a slight but significant lengthening in the S—C bond distances (1.775(2) and 1.784(2) Å) as compared with unbonded thiourea S—C distance, which is in the range 1.71–1.73 Å. This bond weakening is confirmed by the red shift observed in the frequency for the S—C stretching mode (see Section 3.4). C—N bond lengths vary in the range from 1.316(3) to 1.326(3) Å and N—CH_3 distances from 1.463(3) to 1.477(3) Å. The above inter-atomic bond distances, in general, agree with those values previously reported for the cation [21].

The $[N(CH_3)_2]_2C{=}S{-}S{=}C[N(CH_3)_2]_2^{2+}$ ion exhibits a non-crystallographic twofold axis through the mid point of the linking S—S bond (ideal C_2 local symmetry) that

Table 2
Selected intra-molecular bond distances (Å) and angles (°) in $[N(CH_3)_2]_2C{=}S{-}S{=}C[N(CH_3)_2]_2Cl_2 \cdot 2H_2O$

Monomer #1		Monomer #2	
Bond distances			
C(1)—N(11)	1.316(3)	C(2)—N(21)	1.323(3)
C(1)—N(12)	1.326(3)	C(2)—N(22)	1.319(3)
C(1)—S(1)	1.784(2)	C(2)—S(2)	1.775(2)
C(111)—N(11)	1.463(3)	C(211)—N(21)	1.469(3)
C(112)—N(11)	1.467(3)	C(212)—N(21)	1.477(3)
C(121)—N(12)	1.473(3)	C(221)—N(22)	1.475(3)
C(122)—N(12)	1.466(3)	C(222)—N(22)	1.471(3)
	S(1)—S(2)	2.0454(9)	
Bond angles			
N(11)—C(1)—N(12)	123.8(2)	N(21)—C(2)—N(22)	123.2(2)
C(111)—N(11)—C(112)	113.2(2)	C(211)—N(21)—C(212)	114.1(2)
C(122)—N(12)—C(121)	113.6(2)	C(222)—N(22)—C(221)	113.7(2)
	C(1)—S(1)—S(2)	102.66(8)	
	C(2)—S(2)—S(1)	104.71(8)	

relates the two molecular halves of the dimer. This is quantified by the closeness in the corresponding torsion angles along the TMTU monomers (differences of less than 8.5°).

As expected, the SCN_2 skeletons are nearly planar (rms deviations of atoms from the corresponding least-squares planes being less than 0.013 Å). Because of steric repulsion between neighbouring methyl groups, and at variance with the NH_2 planes in TU, the NC_2 groups depart from co-planarity with the corresponding molecular SCN_2 skeletons. In fact, they are tilted around the C—N bonds in angles of 24.7(3) and 30.1(2)° for monomer #1 (dihedral angle between the CN_2 planes of 47.9(3)°) and 14.3(2) and 30.5(2)° for monomer #2 (NC_2 planes angled in 50.1(2)°).

The ionic crystal is further stabilised by Ow—H ··· Cl bonds (Ow ··· Cl distances in the range from 3.196 to 3.335 Å and Ow—H ··· Cl angles from 171.1 to 179.6°). H-bond distances and angles are detailed as supplementary material.

Table 3
Assignment of principal Raman and IR bands of TMFDS chloride

Raman	IR	Calculated	Assignment
152		125	ρ CH_3
217		183	τ CH_3
245		231	τ CH_3
437		419	τ CH_3
471	471	452	ν S—S
537		491	ν S—S + δ (CH_3—N—CH_3)
	618	594	ν S—C + δ N—C—N + δ C—N—C
628		596	ν S—C + δ N—C—N + δ C—N—C
663		671	π C out of plane NSN
	873	860	ν_a N—CH_3
	1062	1055	ν_a (CH_3—N—CH_3) + ρ CH_3
1091	1097	1067	ν_a (CH_3—N—CH_3) + ρ CH_3
	1116	1109	ρ CH_3 + ν_a CS
	1128	1117	ρ (CH_3)
	1166	1161	ρ (CH_3)
	1200	1191	ρ (CH_3)
	1250	1256	δ (NCN) +ν_a N—CH_3+ρ CH_3
1358			ν SC + ν_s CN + δ CH_3
	1407	1407	δ CH_3 + ν_s(CN) + ν_a CS
1410		1408	δ CH_3 + ν_s(CN) + ν_a CS
1431	1456	1447	δ CH_3
1451	1467	1463	δ CH_3
1475		1493	δ CH_3
	1507	1512	δ CH_3
	1558	1547	δ CH_3
	1619	1644	ν_a N—C + δ CH_3
	1634		δ H_2O
2800			ν_s CH
	2849	3072	ν_s CH
2857		3075	ν_s CH
	2918	3161	ν_a CH
2943		3162	ν_a CH
3004		3167	ν_a CH

3.3. DFT structure optimization and normal mode frequencies of the $[N(CH_3)_2]_2C{=}S{-}S{=}C[N(CH_3)_2]_2^{2+}$ ion

The optimisation of the isolated structure of the ion (Fig. 3) was carried out with tight convergence criterion using the 6-311G(d,f) basis set at DFT theory level. The hybrid method B3LYP, Becke 3 parameter exchange functional plus the correlation functional according to Lee, Yang, and Parr, were applied [29]. The molecule was constrained to the C_2 point symmetry with the unique axis orientation normal to the S—S bond vector. Solid state coordinates were used for generating the starting geometry. The harmonic frequencies and the vibration modes for the optimised structure were computed from the diagonalised mass-weighted Hessian matrix. The calculated mode frequencies were used as reference for the assignment of some vibration modes of the experimental spectrum, as discussed in the next section. Both experimental and calculated frequencies are compared in Table 3. As anharmonicity effects were neglected [30], *ab initio* vibrational frequencies are typically larger than the experimental ones. Thus, calculations at B3LYP and BLYP theory levels using the 6-31G(d) basis set yielded scale factors 0.9614 and 0.9945, respectively, and those derived from the BLYP stheory levels using 6-311G(df,p) yielded 0.9986 [30]. Therefore, the frequency values calculated in this work should be scaled down by a factor between 0.96 and 0.99. The program Gaussian03 [31] was used for all calculations.

The computed electron distribution at the ion was used to derive the atomic partial charges by the Mulliken and ESP: Electrostatic potential-derived charges (CHELPG method implemented in G03) methods. The net charge of the ion is +2, therefore it is able to withhold 2 chloride counter-ions in the asymmetric unit of the crystal structure. In both methods the atomic partial charge of the methyl groups is all positive and only a small net charge is left for the sulphur atoms (see Table 4).

3.4. IR and Raman spectroscopy of TMFDS salt

The vibrational spectra of the TMFDS salt is shown in Fig. 4. The assignment of the absorption bands (Table 3) was based on wave numbers obtained from DFT calculations (Section 3.3) and data of similar molecules reported in the literature [32]. The spectrum can be analysed considering six spectroscopic regions. The first one, observed only in

Table 4
Calculated atomic partial charges in the $[N(CH_3)_2]_2C = S{-}S = C[N(CH_3)_2]_2^{2+}$ isolated ion

Atom	S1	S2	N21	N22	N11	N12	C2	C1	C212	C211	C222	C221	C111	C112	C121	C122	H (avg)	Dipole (Dy)
Mulliken	0.29	0.28	−0.47	−0.45	−0.46	−0.47	0.18	0.20	0.37	0.36	0.37	0.36	0.37	0.35	0.37	0.35	0.26(2)	4.65
ESP	0.01	0.03	−0.14	−0.10	−0.11	−0.13	0.29	0.30	0.26	0.21	0.24	0.23	0.23	0.22	0.26	0.20	0.10(4)	4.51

Values of the average hydrogen atoms partial charges and their variances are shown.

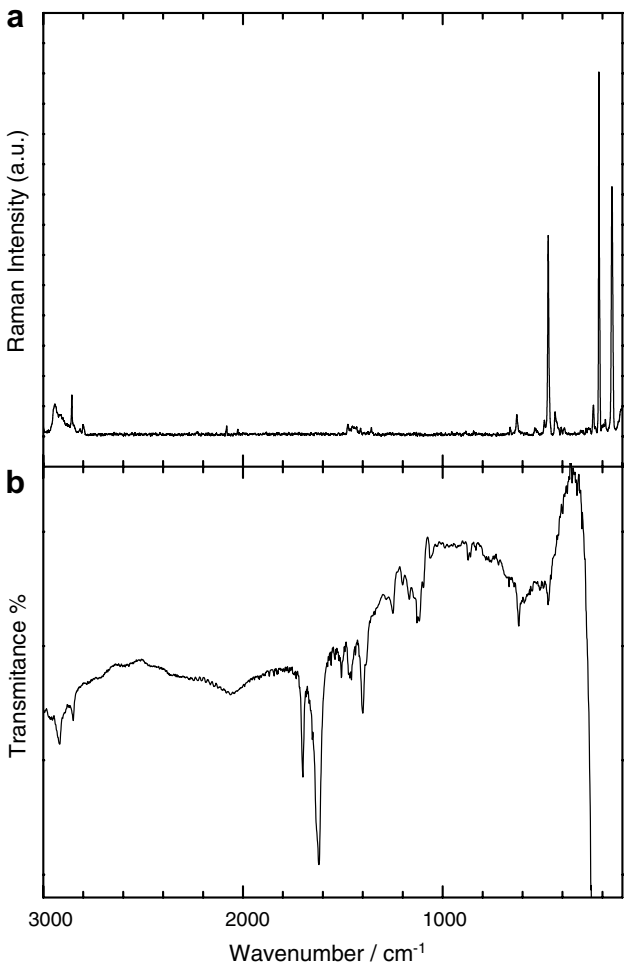

Fig. 4. Raman (a) and IR (b) spectra of TMFDS in KBr.

the Raman spectrum, covers the range 100–400 cm^{-1} and shows two very strong bands at 152 and 217 cm^{-1}. These bands are mainly related to torsions of the CH_3 groups.

The second wave number region covers the range from 400 to 1000 cm^{-1} . For this region, the vibration modes are mainly associated with C—S stretching. The S—S stretching band appears at about 470 cm^{-1} . As expected from the low polarity of this vibration, the intensity of the IR band is considerably weak, whereas the corresponding Raman band is very strong. At 618 (IR) and 628 (Raman) cm^{-1} the asymmetric and symmetric C–S stretching bands, respectively, appear. Moreover, the Raman spectrum also shows a weak band at 663 cm^{-1} that can be assigned to the C out of plane NSN deformation. Finally, the two weak bands observed at 861 and 873 cm^{-1} are assigned to the bending and the stretching modes of the N—C bond, respectively.

The wave number range from 1000 to 1400 cm^{-1} involves complex vibration modes. The main contributions to these modes are the CH_3-rocking, the N—C—N bridge bending and the stretching of the N—CH_3, C—N and S—C bonds.

In the range from 1400 to 1700 cm^{-1} a strong IR band at 1407 cm^{-1} is observed. This can be assigned to the combination of S—C stretching, C—N symmetric stretching and CH_3 bending. Afterwards, a series of weaker bands mainly related to the bending of the CH_3 groups is recorded.

At 1619 cm^{-1} the IR spectrum exhibits a very strong band overlapped by another strong band centred at 1634 cm^{-1}. Both bands are assigned to the asymmetric stretching of the N—C—N bridge. According to DFT calculations, the first band is associated with a transition dipole derivative vector nearly perpendicular to the molecular two-fold axis, while for the second band the dipole vector appears to be nearly parallel to this symmetry axis. An IR band is observed at 1700 cm^{-1}, but this should be related to the presence of an impurity in the compound, likely a carbonyl-containing species. The stretching of the CO bond in carbonyl compounds commonly appears at around 1700 cm^{-1}, and considering that the synthesis of the compound utilises hydrogen peroxide, a very powerful oxidising agent, it is reasonable to assume that a small amount of TMTU is oxidised to a higher state than that of the disulphide. This also agrees with the electrochemical results showing that at relatively high potentials, i.e. 1.4–1.6 V, the presence of CO-containing species in the solution is detected (Fig. 2).

Finally, in the range 2800–3000 cm^{-1}, two IR bands at 2849 and 2918 cm^{-1} are observed. They can be assigned to the symmetric and asymmetric stretching modes of the CH bonds, respectively.

3.5. Comparison of the electrochemical and the homogeneous chemical formation of $[TMFDS]^{2+}$ ions

3.5.1. Likely electrochemical reaction pathway

The voltammetry of TMTU on platinum in acid solutions under quiescent condition (Fig. 1a), in the potential range 0.1–0.8 V, is related to the following redox couple

$$2\mathrm{TMTU(sol)} \rightleftharpoons [\mathrm{TMFDS}]^{2+} + 2e^- \quad (1)$$

This process behaves as an electrochemical reaction under diffusion control [33]. On the other hand, similar runs with the rotating disc electrode (Fig. 1b) demonstrate a slight enhancement of the anodic reaction between 0.4 and 0.45 V, and a certain inhibition for $E > 0.5$ V. The latter indicates that reaction (1) in both directions behaves as a complex process in which the formation of soluble $TMFDS^{2+}$ simultaneously occurs with the appearance of surface species that partially inhibit the anodic reaction (compare Fig. 1a and 1b). Moreover, for the reverse reaction the inhibiting effect is enhanced.

It is known that TMTU adsorbs on platinum, the corresponding adsorption free energy at 298 K being $\Delta G_{ads} \approx -40$ kJ mol^{-1} [34], i.e. the adsorption of TMTU on platinum is moderately strong, and it already occurs from about 0.02 V to 0.3 V, and the electrosorption of TMTU undergoes between 0.3 and 0.5 V or thereabouts,

i.e. in the potential range where a small anodic current is recorded (Fig. 1b). Therefore, the electrosorption commences at a potential that is close to the potential of total zero charge of platinum in acid solutions [35,36]. The TMTU/Pt interaction at $E < 0.05$ V is beyond the scope of this work.

The pseudo-capacitance (C_s) related to the electrosorption process can be estimated from the voltammetric data under rotation conditions from the relationship $C_s = I\ v/A$, where I is the anodic current read at 0.4 V, A is the electrode area and v is the potential scan rate. The value of $C_s \approx 100\ \mu F\ cm^{-2}$ indicates a platinum surface partially covered by the electroadsorbed species. Considering that the pseudo-capacitance for an adsorbate monolayer, each adsorbate occupying a single surface site, is about $1500\ \mu F\ cm^{-2}$ [37], and the TMTU adsorbate is almost flat on the surface covering about 9–10 sites, it results that for the conditions of our work the platinum surface is covered about 60%. Accordingly, considering that the main product from the first electro-oxidation stage is detected and identified in the range 0.4–0.8 V, the corresponding partial inhibition of the anodic reaction is likely related to the formation of an adsorbate that behaves as an intermediate in dimer formation. Therefore, reaction (1) should occur via a consecutive reaction pathway where TMTU molecules reach the reaction interface by diffusion from the bulk of the solutions to the electrochemical interface (e.i.) where they are electro-oxidised to $TMTU^+$ adsorbates via a single electron transfer process. Subsequently, the second electron transfer results from the reaction and desorption of $TMTU^+$ with another soluble TMTU molecule at the electrode interface, yielding $TMFDS^{2+}$ ions in solution,

$$TMTU(sol) \rightarrow (TMTU)_{e.i.} \quad (2)$$

$$Pt(s) + (TMTU)_{e.i.} \rightarrow (TMTU^+)_{ad}Pt(s) + e^- \quad (3)$$

$$(TMTU^+)_{ad}Pt(s) + TMTU(sol) \rightarrow [TMFDS]^{2+}(aq) + Pt(s) + e^- \quad (4)$$

step (2), the adsorption of TMTU is diffusion controlled; step (3), the formation of $TMTU^+$ adsorbate behaves as a quasi-reversible electron transfer, as has been found by modulated voltammetry for TMTU electro-oxidation on gold electrodes [38]; step (4) represents the fast formation of the soluble TMTU dimer ($TMFDS^{2+}$) via a second-order reaction. Thus, the rate of the overall reaction is determined by the TMTU diffusion rate from the bulk of the solution interfered by the partial coverage of the platinum surface by $TMTU^+$ adsorbates.

It should be noted that the stability of $TMTU^+$ adsorbates at potentials where the platinum surface is positively charged should be assisted by co-adsorption of sulphate/bisulphate ions, as has been concluded from platinum single-crystal electrodes in sulphate-containing media [39]. The electrochemical formation of soluble $[TMFDS]^{2+}$ is confirmed by the appearance of the IR band of the solid compound at $1623\ cm^{-1}$, as shown above.

As far as the electroreduction of the dimer ion is concerned, a process that is followed under still solution (Fig. 1a) can be represented as follows

$$[TMFDS]^{2+}(aq) + Pt(s) + e^- \rightarrow (TMTU^+)_{ad}Pt(s) + TMTU(aq) \quad (5)$$

$$(TMTU^+)_{ad}Pt(s) + e^- \rightarrow TMTU + Pt(s) \quad (6)$$

$$(TMTU)_{e.i.} \rightarrow TMTU(sol) \quad (7)$$

3.5.2. $[TMFDS]^{2+}$ free energy formation for the heterogeneous and the homogeneous reaction

As reported above, the same dimer ($[TMFDS]^{2+}$) can be produced either by homogeneous chemical oxidation or heterogeneous electro-oxidation. Therefore, it is interesting to compare the free energies of dimer ion formation from both the electrochemical and the chemical processes. The dimer ion is obtained by chemical reaction between aqueous 0.4 M TMTU and 0.20 M H_2O_2 + 0.49 M HCl. The overall redox process consists of

$$2TMTU(aq) \rightarrow [TMFDS]^{2+}(aq) + 2e^- \quad (8)$$

$$H_2O_2(aq) + 2H^+(aq) + 2e^- \rightarrow 2H_2O(aq) \quad (9)$$

The initial driving force of the overall reaction, ΔG_r, results from the difference in the reversible potential of reactions (8 and 9). For reaction (8) the value of E_r, which is estimated from the anodic and cathodic half-wave potentials, results in 0.5 ± 0.05 V, whereas for reaction (9) from the Nernst equation [40] it results in 1.39 ± 0.10 V, a figure that is about 0.5 V higher than the threshold potential for TMTU electro-oxidation on platinum (Fig. 1a). The value of $E_{r,8}$ is close to that reported for several thioureas/dimer redox couples [18].

Accordingly, chemical dimer formation can be expressed by the sum of the partial reactions 8 and 9,

$$2TMTU(aq) + H_2O_2(aq) + 2H^+(aq) = [TMFDS]^{2+}(aq) + 2H_2O(aq) \quad (10)$$

and under the initial conditions of our experiments, the value of $\Delta G_{r,10}$ is

$$\Delta G_{r,10} = -2F(E_{r,9} + E_{r,8}) = -172\ kJ\ mol^{-1} \quad (11)$$

F being the Faraday and 2 the number of electrons involved per dimer ion formation.

On the other hand, the maximum dimer electrochemical formation rate, which occurs at the anodic current peak Ia that appears at 0.70 V (Fig. 1a), results in $\Delta G_{r,8} \approx 135\ kJ\ mol^{-1}$. Besides the enthalpy and entropy contributions, this figure involves the contribution of the applied electric potential. Therefore, the difference in ΔG_r between the heterogeneous and the homogeneous processes is ca. $37\ kJ\ mol^{-1}$.

According to the transition state theory [41], the rate ratio of the homogeneous and heterogeneous second-order processes (v_{hete}/v_{homo}) approaches the proportionality

$$v_{hete}/v_{homo} \approx c_s/F_{\#} \exp[(\Delta G_{r,8} - \Delta G_{r,10})/RT] \quad (12)$$

c_s and $F_{\#}$ being the concentration of active surface sites per cm^2, and the partition function of the activated complex, respectively. Thus, for reactions in solution for which $c_s \approx 10^{15}$ sites cm^{-2} and $10^{27} \leqslant F_{\#} \leqslant 10^{28}$ [41], a pre-exponential factor of the order of 10^{-12}–10^{-13} should be expected. Then, considering that in our case the exponential term is of the order of 10^{13} it follows that:

$$v_{hete}/v_{homo} \approx 1 \quad (13)$$

This figure indicates that the maximum rate of both the chemical and the electrochemical reactions occurs under a comparable driven force. This conclusion is consistent with the common formation of the dimer ion as well as carbonyl-containing species as side products from both reactions (Figs. 2 and 4).

4. Conclusions

The TMFDS was prepared by electro-oxidation of TMTU on platinum in aqueous perchloric acid and by chemical oxidation of TMTU utilising hydrogen peroxide in hydrochloric acid medium. The TMFDS was characterised by IR and Raman spectroscopy and the crystal structure of the chloride salt determined by X-ray diffractometry. The two molecular halves of the dimer are linked by a disulphide single bond and related to each other by a non-crystallographic pseudo two fold axis. The comparison of the IR and FTIRRAS confirms the formation of TMFDS by either chemical or electrochemical processes. The maximum rate of both homogeneous and heterogeneous processes occurs under comparable driving forces. This is consistent with the common formation of the dimer ion as well as carbonyl-containing species as side products in both reactions.

Acknowledgements

This work was supported by ANPCYT (PICT 12508/02), CONICET (Argentina) and FAPESP (Brazil). AEB thanks Prof. T. Iwasita at the Instituto de Quimica de São Carlos (Brazil) for generously providing FTIRRAS facilities. AEB is member of the Research Career of CICPBA.

Appendix A. Supplementary data

Crystallographic data (excluding structure factors) have been deposited with the Cambridge Crystallographic Data Centre, CCDC No. 617730. Copies of this information may be obtained free of charge from www.ccdc.cam.ac.uk/conts/retrieving.html (or from the Cambridge Crystallographic Data Centre (CCDC), 12 Union Road, Cambridge CB2 1EZ, UK; fax: +44 1223 336033; e-mail: deposit@ccdc.cam.ac.uk). Supplementary data associated with this article can be found, in the online version, at doi:10.1016/j.molstruc.2007.02.004.

References

[1] E.E. Reid, Organic Chemistry of Bivalent Sulfur, vol. 5, Chemical Publishing Co., New York, 1963.
[2] P.A.S. Smith, Open-Chain Nitrogen Compounds, W.A. Benjamin, New York, 1965.
[3] D. Pletcher, F. Walsh, Industrial Electrochemistry, Chapman and Hall Ltd., London, 1990.
[4] A. Szymaszek, J. Biernat, L. Pajdowski, Electrochim. Acta 22 (1977) 359.
[5] D.F. Suarez, F.A. Olson, J. App. Electrochem. 22 (1992) 1002.
[6] E.E. Farndon, F.C. Walsh, S.A. Campbell, J. App. Electrochem. 25 (1995) 574.
[7] V.S. Martín, S. Sanllorente, S. Palmiero, Electrochim. Acta 44 (1998) 579.
[8] D.N. Upadhayay, V. Yegnaraman, Mat. Chem. Phys. 62 (2000) 247.
[9] R. Agrawal, T.K.G. Namboodhiri, Corrosion science 30 (1990) 37.
[10] G.R. Dey, D.B. Naik, K. Kishore, P.N. Moorthy, Radiat. Phys. Chem. 43 (1994) 365.
[11] G.R. Dey, D.B. Naik, K. Kishore, P.N. Moorthy, J. Chem. Soc. Perkin Trans. 2 (1994) 1625.
[12] B. Pesic, T. Seal, Metall. Trans. 21B (1990) 419.
[13] T. Kai, T. Hagiwara, H. Haseba, T. Takahashi, Ind. Eng. Chem. Res. 36 (1997) 2757.
[14] S. Aguayo Salinas, M.A. Encinas Romero, I. González, J. Appl. Electrochem. 28 (1998) 417.
[15] J. Li, J.D. Miller, Hydrometallurgy 63 (2002) 215.
[16] E. Bunge, S.N. Port, B. Roelfs, H. Meyer, H. Baumgärtel, D.J. Schiffrin, R.J. Nichols, Langmuir 13 (1997) 85.
[17] O.E. Piro, E.E. Castellano, R.C.V. Piatti, A.E. Bolzán, A.J. Arvia, Acta Cryst. C58 (2002) 252.
[18] M. Hoffmann, J.O. Edwards, Inorg. Chem. 16 (1977) 3333.
[19] U. Bierbach, W. Barklage, W. Saak, S. Pohl, Z. Naturforsch. 47b (1992) 1593.
[20] A.E. Bolzán, P. Schilardi, R.C.V. Piatti, T. Iwasita, A. Cuesta, C. Gutiérrez, A.J. Arvia, J. Electroanal. Chem. 571 (2004) 59.
[21] H. Senda, S. Kitoh, T. Suganami, K. Kunimoto, Anal. Sciences 16 (2000) 1003.
[22] Enraf-Nonius (1997–2000). COLLECT. Nonius BV, Delft, The Netherlands.
[23] Z. Otwinowski, W. Minor, in: J.C.W. Carter, R. Sweet (Eds.), Methods in Enzymology, Academic Press, New York, 1997, pp. 307–326.
[24] G.M. Sheldrick, SHELXS-97 Program for Crystal Structure Resolution, University of Göttingen, Göttingen, Germany, 1997.
[25] G.M. Sheldrick, SHELXL-97 Program for Crystal Structures Analysis, University of Göttingen, Göttingen, Germany, 1997.
[26] C.K. Johnson, ORTEP-II. A Fortran Thermal-Ellipsoid Plot Program, Report ORNL-5318, Oak Ridge National Laboratory, Tennessee, USA, 1976.
[27] A.E. Bolzán, I.B. Wakenge, R.C. Salvarezza, A.J. Arvia, J. Electroanal. Chem. 475 (1999) 181.
[28] U. Anthoni, P.H. Nielsen, G. Borch, J. Gustavsen, P. Klaboe, Spectrochim. Acta Part A 33 (1977) 403.
[29] P.J. Stephens, J.F. Devlin, C.F. Chabalowski, M.J. Frisch, J. Phys. Chem. 98 (1994) 11623.
[30] A.P. Scott, L. Radom, J. Phys. Chem. 100 (1996) 16502.
[31] R.B.M.J. Frisch, G.W. Trucks, H.B. Schlegel, G.E. Scuseria, M.A. Robb, J.R. Cheeseman, J.A. Montgomery, Jr., T. Vreven, K.N. Kudin, J.C. Burant, J.M. Millam, S.S. Iyengar, J. Tomasi, V. Barone, B. Mennucci, M. Cossi, G. Scalmani, N. Rega, G.A. Petersson, H. Nakatsuji, M. Hada, M. Ehara, K. Toyota, R. Fukuda, J. Hasegawa, M. Ishida, T. Nakajima, Y. Honda, O. Kitao, H. Nakai, M. Klene, X. Li, J.E. Knox, H.P. Hratchian, J.B. Cross, C. Adamo, J. Jaramillo, R.

Gomperts, R.E. Stratmann, O. Yazyev, A.J. Austin, R. Cammi, C. Pomelli, J.W. Ochterski, P.Y. Ayala, K. Morokuma, G.A. Voth, P. Salvador, J.J. Dannenberg, V.G. Zakrzewski, S. Dapprich, A.D. Daniels, M.C. Strain, O. Farkas, D.K. Malick, A.D. Rabuck, K. Raghavachari, J.B. Foresman, J.V. Ortiz, Q. Cui, A.G. Baboul, S. Clifford, J. Cioslowski, B.B. Stefanov, G. Liu, A. Liashenko, P. Piskorz, I. Komaromi, R.L. Martin, D.J. Fox, T. Keith, M.A. Al-Laham, C.Y. Peng, A. Nanayakkara, M. Challacombe, P.M.W. Gill, B. Johnson, W. Chen, M.W. Wong, C. Gonzalez, J.A. Pople, Gaussian Inc., Pittsburgh PA.

[32] H. Günzler, H.-U. Gremlich, IR Spectroscopy, Wiley-VCH Verlag GmbH, Weinheim, 2002.

[33] A.J. Bard, L.R. Faulkner, Electrochemical Methods, J. Wiley and Sons, New York, 1980.

[34] A.E. Bolzán, R.C.V. Piatti, R.C. Salvarezza, A.J. Arvia, J. Appl. Electrochem. 32 (2002) 611.

[35] K.J.J. Mayrhofer, B.B. Blizanne, M. Arenz, V.R. Stamenkovic, P.N. Ross, N.N. Markovic, J. Phys. Chem. B 109 (2005) 14433.

[36] S. Trasatti, E. Lust, vol. 33, Plenum Press, New York, 1999.

[37] S. Srinivasan, E. Gileadi, Electrochim. Acta 11 (1966) 321.

[38] A.E. Bolzán, T. Iwasita, A.J. Arvia, Electrochim. Acta 51 (2005) 1044.

[39] O.M. Magnussen, Chem. Rev. 102 (2002) 679.

[40] A. Bard, R. Parsons, R. Jordan (Eds.), Standard Potentials in Aqueous Solutons, IUPAC/M. Dekker, New York and Basel, 1985.

[41] S. Glasstone, K.J. Leidler, H. Eyring, The Theory of Rate Processes, McGraw-Hill, New York, 1941.